Stochastic model of organizational state transitions in a turbulent pipe flow

R. Jäckel [1,3] B. Magacho [2,3] B. Owolabi [2,3] L. Moriconi [2,3,*]
D. J. C. Dennis [3] and J. B. R. Loureiro [1,3]

[1]*Programa de Engenharia Mecânica, Coordenação dos Programas de Pós-Graduação em Engenharia, Universidade Federal do Rio de Janeiro, C.P. 68503, 21941-972 Rio de Janeiro, RJ, Brazil*
[2]*Instituto de Física, Universidade Federal do Rio de Janeiro, Av. Athos da Silveira Ramos 149, 21941-909 Rio de Janeiro, RJ, Brazil*
[3]*Interdisciplinary Center for Fluid Dynamics, Universidade Federal do Rio de Janeiro, R. Moniz Aragão 360, 21941-594 Rio de Janeiro, Brazil*

Turbulent pipe flows exhibit organizational states (OSs) that are labeled by discrete azimuthal wave number modes and are reminiscent of the traveling wave solutions of low Reynolds number regimes. The discretized time evolution of the OSs, obtained through stereoscopic particle image velocimetry, is shown to be non-Markovian for data acquisition carried out at a structure-resolved sampling rate. In particular, properly defined time-correlation functions for the OS transitions are observed to decay as intriguing power laws, up to a large-eddy time horizon, beyond which they decorrelate at much faster rates. We are able to establish, relying upon a probabilistic description of the creation and annihilation of streamwise streaks, a lower-level *Markovian* model for the OS transitions, which reproduces their time-correlated behavior with meaningful accuracy. These findings indicate that the OSs are distributed along the pipe as statistically correlated packets of quasistreamwise vortical structures.

I. INTRODUCTION

Notwithstanding the large body of knowledge accumulated since the landmark experiments of Reynolds [1], turbulent pipes comprise flow patterns which have remained surprisingly unsuspected until recent years. They can be depicted as relatively organized sets of wall-attached low-speed streaks coupled to pairs of counterrotating quasistreamwise vortices [2–4]. These *organizational states* (OSs) actually characterize the turbulent velocity fluctuations at high Reynolds numbers and are topologically similar to traveling waves—a class of exact (but unstable) low-Reynolds number solutions of the Navier-Stokes equations [5–7].

As for traveling waves, the OSs can be classified by the number of low-speed streaks they contain. Observation tells us, however, that this quantity changes in an apparently random way along the turbulent pipe. For the sake of illustration, Fig. 1 shows a transition between OSs, visualized from a pair of cross-sectional snapshots of the flow obtained through stereoscopic particle image velocimetry (sPIV).

The existence of spatial transitions among the OS modes suggests, within the perspective of dynamical systems, that the turbulent pipe flow could be described as a chaotic attractor and its unstable periodic orbits in a phase space of much reduced dimensionality [8–12]. In connection
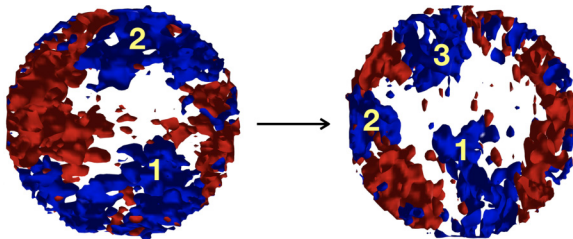
---

*moriconi@if.ufrj.br

FIG. 1. Example of a transition between organizational states, as sampled out from our measurements, which are associated with two and three low-speed streaks. Blue and red refer, respectively, to negative and positive streamwise velocity fluctuations around the mean. The systematic procedure to ascertain a well-defined number of low-speed structures to a given flow snapshot is discussed in the text.

with this circle of ideas, we are motivated to study the OS transitions in the framework of stochastic processes, focusing particular attention on their recurrent dynamics.

This paper is organized as follows. We highlight in Sec. II the main methodological aspects related to the classification and detection of the OS modes. In Sec. III their transitions are investigated from the point of view of stochastic processes. A standard statistical test (reported in an Appendix) shows that the transitions between OS modes do not form a Markov chain. In order to explore the time recurrence of states and transitions, we introduce correlation functions which unveil the existence of a peculiar hidden self-similar behavior of the OS mode fluctuations. Next, in Sec. IV we recover some of the essential results of the previous section, addressing the OS mode transitions as a high-level (non-Markovian) description of a more fundamental low-level Markovian stochastic process. Finally, in Sec. IV we summarize our findings and point out directions of further research.

II. ORGANIZATIONAL STATES: CLASSIFICATION AND DETECTION

To start, let $u = u(r, \theta)$ be in polar coordinates the fluctuating streamwise component of the velocity field defined over a fixed pipe's cross-sectional plane. We may introduce accordingly the instantaneous spectral power density,

$$I(k_n) = \int_0^{2\pi} d\theta e^{ik_n\theta} f_{uu}(r_0, \theta), \tag{2.1}$$

where

$$f_{uu}(r_0, \theta) = \int_0^{2\pi} d\theta' u(r_0, \theta') u(r_0, \theta' + \theta), \tag{2.2}$$

$k_n = n \in \mathbb{Z}^+$ is an azimuthal wave number, and r_0 is a reference radial distance which falls within the log region of the pipe's turbulent boundary layer. In order to probe low-speed streaks as close as possible to the pipe's surface and avoid spurious bulk effects, the value of r_0 is taken to be $\approx 80\%$ of the pipe's radius (sPIV measurements are affected by lack of resolution for $r > 0.8R$, so this region is completely discarded in our statistical analyses). Empirical evidence shows that $I(k_n)$ is in general peaked at some clearly dominant wave number k^* (to be identified to the number of snapshot low-speed streaks), which can be used to label the probed velocity profile $u(r, \theta)$.

For the purpose of concreteness, Fig. 2 shows the power spectrum for a snapshot of the OS mode $k_n = 4$. We note that the dominant peak in the spectral density $I(k_n)$ is not always as prominent as in Fig. 2, and other Fourier modes can sometimes be nearly as important as the dominant mode.

We also remark, to avoid (tempting) misconceptions, that the selected dominant OS modes may not dominate the cross-sectional flow energy (that is, $u^2 + v^2 + w^2$ integrated over the entire pipe's cross section). All we can assume, on more precise grounds, is that the dominant OS mode contains most of the streamwise kinetic energy *restricted* to a radial range which partially comprises the
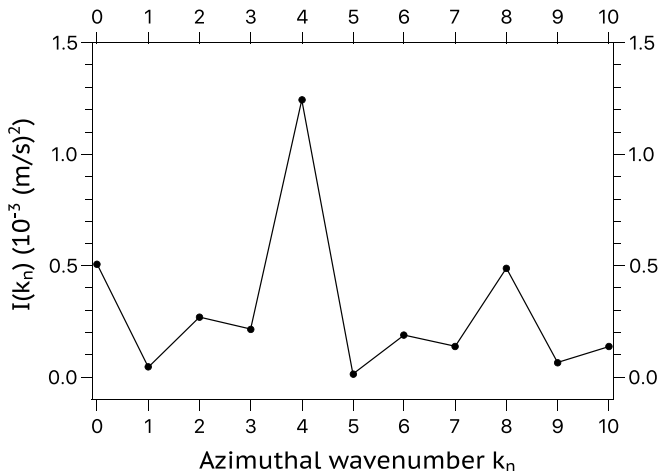
FIG. 2. Power spectrum for a given sPIV snapshot of the flow, as evaluated from Eq. (2.1). The streamwise velocity field is in this instance dominated by the wave number $k^* = 4$.

inner boundary layer. For the case illustrated in Fig. 2, we find that the single wave number $k^* = 4$ supports, for $0.6 \leqslant r/R \leqslant 0.8$, about 32% of the streamwise kinetic energy that flows through that annular region.

As time evolves, $I(k_n)$ changes, and so does the wave number position of its dominant peak. Therefore, if $u(r, \theta)$ is recorded at equally spaced time intervals Δ, the dynamical evolution of the pipe turbulent field can be mapped into the stochastic process

$$\mathcal{S} \equiv \{k^*(t), k^*(t + \Delta), k^*(t + 2\Delta), \ldots\}. \tag{2.3}$$

In order to investigate the still very open statistical properties of $\mathcal{S}$, we have performed a pipe flow experiment, at Reynolds number Re $= 24\,415$, in the large pipe rig facility of the Interdisciplinary Nucleus for Fluid Dynamics (NIDF) at the Federal University of Rio de Janeiro. The pipe's diameter and length are, respectively, $D = 15$ cm and $L = 12$ m. By means of sPIV, with sampling rate of 10 Hz (i.e., $\Delta = 0.1$ s), we have collected 10^4 cross-sectional snapshots of the flow, each one containing the three components of the turbulent velocity field over a uniform grid of size 78×78. It turns out that essentially all the observed OS modes fall into the range $0 \leqslant k^* \leqslant k^*_{\max} = 10$.

Our experimental data have been validated with the help of previous benchmark pipe flow experiments [13] through the inspection of the performance of first- and second-order single-point statistics for the streamwise component of velocity field. We have also attained a further validation of the entire measured velocity field, from the evaluation of particularly defined streamwise velocity-velocity correlation functions conditioned on the OS modes k^*, more precisely,

$$R_{uu}(\Delta \mathbf{r}|k^*) \equiv \mathbb{E}[u(\mathbf{r}_0)u(\mathbf{r}_0 + \Delta \mathbf{r})|k^*], \tag{2.4}$$

which has its level curves depicted in Fig. 3, for the case $k^* = 5$, in close correspondence with known results [4]. The above conditional average is taken over all the sPIV snapshots that are labeled by the same dominant wave number k^*. A further azimuthal average is carried out as well, over rotations of the cross-sectional streamwise velocity field around the pipe's symmetry axis.

For a discussion of additional measurements and experimental details, we draw the reader's attention to Ref. [14] for a comprehensive account.
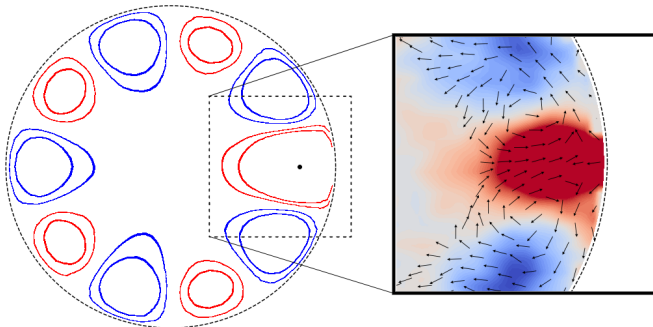
FIG. 3. Statistical results for the OS mode $k^* = 5$. Left image: positive (red) and negative (blue) level curves of R_{uu}, defined by $|R_{uu}(\mathbf{r} - \mathbf{r}_0|k^*)| = 5\%$ and 10% of $(R_{uu})_{\text{max}}$, with the reference point $\mathbf{r}_0$ depicted as a black dot. Right image: a closer look at the averaged streamwise velocity fluctuations (red for positive, blue for negative), conditioned on $u(\mathbf{r}_0) > 0$. The cross-sectional averaged velocity field reveals the vortical structures that are usually coupled with velocity streaks.

III. ORGANIZATIONAL STATE TRANSITIONS AS A STOCHASTIC PROCESS

The first immediate question that can be raised about the stochastic process $\mathcal{S}$ is whether it is Markovian or not, that is, whether its state probabilities are independent of the past, making the system effectively memoryless. A standard statistical test, reported in the Appendix, indicates in a straightforward way that $\mathcal{S}$ is not Markovian.

It is reasonable to expect, however, that the decimated process for large enough time lags is essentially Markovian, since in this situation the OS modes become weakly correlated. The transition to Markovian behavior can be alternatively addressed from the analysis of correlation functions, which we introduce as it follows. Taking $0 \leqslant m, m' \leqslant k^*_{\text{max}}$, let $V_m(t)$ and $M_{m'm}(t)$ be, respectively, the components of a vector $\mathbf{V}(t)$ and a matrix $\mathbf{M}(t)$, both derived from $\mathcal{S}$ as

$$V_m(t) = \begin{cases} 1, & \text{if } k^*(t) = m \\ 0, & \text{otherwise} \end{cases} \tag{3.1}$$

and

$$M_{m'm}(t) = \begin{cases} 1, & \text{if } k^*(t) = m \text{ and } k^*(t + \Delta) = m' \\ 0, & \text{otherwise.} \end{cases} \tag{3.2}$$

From $\mathbf{V}(t)$ and $\mathbf{M}(t)$ we may find which are the OS modes and the transitions that take place at time instant t. As an instructive example of the above definitions, take $k^*_{\text{max}} = 5$ and

$$\mathbf{V}(t) = \begin{bmatrix} 0 \\ 1 \\ 0 \\ 0 \\ 0 \end{bmatrix}, \quad \mathbf{M}(t) = \begin{bmatrix} 0 & 0 & 0 & 0 & 0 \\ 0 & 0 & 0 & 0 & 0 \\ 0 & 1 & 0 & 0 & 0 \\ 0 & 0 & 0 & 0 & 0 \\ 0 & 0 & 0 & 0 & 0 \end{bmatrix}. \tag{3.3}$$

We infer, from (3.3), that the OS mode $m = 2$, recorded at time t, changed to $m' = 3$ at time $t + \Delta$. It is clear that $\mathbf{V}(t)$ in fact can be obtained from $\mathbf{M}(t)$, since the only nonvanishing row of the latter is, as a rule, the transpose of the former. Define now the correlation functions

$$\tilde{F}(t - t') \equiv \mathbb{E}[\mathbf{V}(t) \cdot \mathbf{V}(t')] - (\mathbb{E}[\mathbf{V}])^2, \tag{3.4}$$

$$\tilde{G}(t - t') \equiv \text{Tr}\{\mathbb{E}[\mathbf{M}^T(t)\mathbf{M}(t')] - \mathbb{E}[\mathbf{M}]^{\mathbf{T}}\mathbb{E}[\mathbf{M}]\}, \tag{3.5}$$
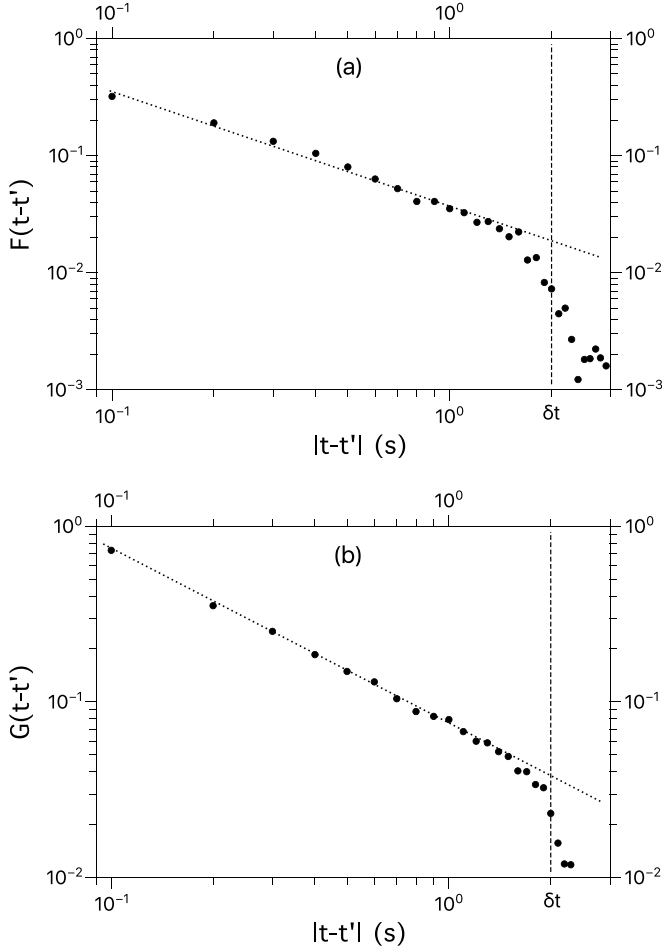
FIG. 4. The time-dependent correlation functions defined in (3.6) are noticed to decay as power laws for $|t - t'| \lesssim \delta t \approx 2$ s. The dotted lines in (a) and (b) have scaling exponent -1 for both $F(t - t')$ and $G(t - t')$.

and their normalized versions,

$$F(t - t') \equiv \frac{\tilde{F}(t - t')}{\tilde{F}(0)}, \quad G(t - t') \equiv \frac{\tilde{G}(t - t')}{\tilde{G}(0)}. \tag{3.6}$$

The functions $F(t - t')$ and $G(t - t')$ describe, respectively, the correlations of *returning* OS modes and transitions which are separated from each other by the time interval $|t - t'|$. Actually, note that $\mathbf{V}(t) \cdot \mathbf{V}(t')$ and $\text{Tr}[\mathbf{M}^T(t)\mathbf{M}(t')]$ are nonvanishing only if, respectively, the OS *modes* and OS *mode transitions* observed at times t and t' are the same. Both definitions (3.4) and (3.5) are motivated, in this sense, from the assumption that unstable periodic orbits play a fundamental role in the description of turbulent pipe flow dynamics [8–12].

The correlation functions $F(t - t')$ and $G(t - t')$ are plotted in Fig. 4 and are noticed to have interesting power-law decays (with the same approximate scaling exponent -1) up to $|t - t'| \equiv \delta t \approx 20\Delta = 2$ s, which suggests some sort of self-similarity across the spatial distribution of about ten OS modes (their mean lifetime is 0.2 s $\approx \delta t/10$). For time separations larger than δt, the correlation functions become undersampled.

Reasoning in terms of the integral (large eddy) timescale of the flow, D/U, where U is the bulk flow velocity, we point out that $\delta t \approx 2D/U$, which suggests that the spatial extension of the self-similar group of OS modes scales with the flow's outer units.

IV. UNDERLYING MARKOVIAN MODEL

It is worth emphasizing that the non-Markovian nature of the stochastic process $\mathcal{S}$ does not mean at all that it cannot be modeled as a Markov process defined in terms of lower-level state variables.

We can render this point more palatable by briefly digressing on a simple example. Consider a stochastic process which has four "microscopic" (i.e., low-level) states labeled as a_1, a_2, a_3, and a_4. States a_1 and a_2 are associated with a single "macroscopic" (i.e., high-level) state A, while a_3 and a_4 are, in their turn, both the degenerate microstates of another macrostate B. Suppose now that transitions between these four microstates define a Markov process, with transition probabilities $p(a_i \rightarrow a_j)$, with $i, j \in \{1, 2, 3, 4\}$.

Taking $p(a_i, n)$ to be the probability to observe the microstate a_i at discretized time instant n (an integer number), we have

$$P(A, n) = p(a_1, n) + p(a_2, n), \tag{4.1}$$

$$P(B, n) = p(a_3, n) + p(a_4, n), \tag{4.2}$$

for the probabilities that the macrostates A and B be observed at the time instant n, respectively. Resorting, furthermore, to the Markov chain relation,

$$p(a_i, n) = \sum_{j=1}^{4} p(a_j, n - 1) p(a_j \rightarrow a_i), \tag{4.3}$$

it is not difficult to show, from Eqs. (4.1)–(4.3) that, in general,

$$P(A, n) \neq P(A, n - 1)P(A \rightarrow A) + P(B, n - 1)P(B \rightarrow A), \tag{4.4}$$

$$P(B, n) \neq P(B, n - 1)P(B \rightarrow B) + P(A, n - 1)P(A \rightarrow B), \tag{4.5}$$

where $P(A \rightarrow A)$, $P(B \rightarrow A)$, etc., are the transition probabilities for the reduced stochastic process given by the macrostates A and B. We conclude, from (4.4) and (4.5), that the transitions between states A and B are not expected to be Markovian, since the state probabilities are not given by the preceding time alone.

To build a bridge to the problem of OS transitions, we first notice that low-speed streaks are created around angular positions of the pipe's cross section which are not necessarily equally spaced (this is actually hinted by the snapshots of Fig. 1). As a matter of fact, positional fluctuations of low-speed streaks are commonly observed during an OS mode life span. The almost perfectly symmetric profiles of OS modes, as the one shown in Fig. 3, are, in contrast, the result of statistical averages.

We assume, thus, that when the creation of a given OS mode $k^* = m$ comes into play, the whole group of its m wall-attached low-speed streaks may be labeled into

$$\Omega(k^*_{\max}, m) = \binom{k^*_{\max}}{m} \tag{4.6}$$

different ways (microstate degeneracy), meaning that the pipe's cross-sectional plane is taken to hold at most $k^*_{\max}$ active low-speed *streak channels*. The phenomenological ground for the introduction of low-speed streak microstates is that they initially appear as small turbulent perturbations at any possible place over the pipe's surface, which can then be azimuthally partitioned into $k^*_{\max}$ equally sized sectors. These are, in other words, the streak channels, angular positions around which the low-speed streaks are centered. Figure 5 illustrates the idea, taking advantage of the same sPIV snapshot that leads to the power spectrum reported in Fig. 2.
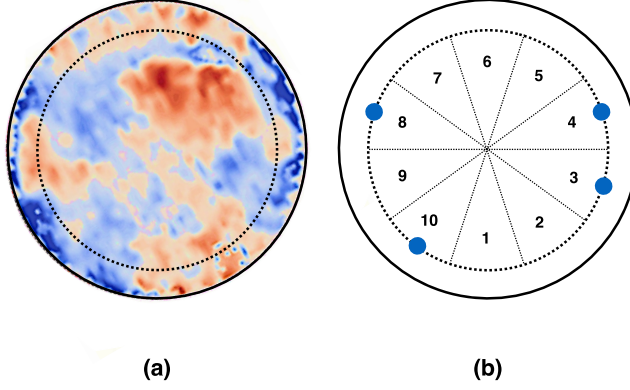
FIG. 5. The sPIV snapshot in (a) gives the power spectrum of Fig. 2. The reference radial distance used in Eq. (2.1), r_0, is the radius of the dotted circle, which essentially crosses the streamwise velocity profile in four disconnected regions that contain low-speed streaks (red spots). Partitioning the snapshot into $k^*_{\mathrm{max}} = 10$ slices, we schematically represent in (b) the positions of the low-speed streaks as small blue dots (the active streak channels are hence labeled as 3, 4, 8, and 10).

The phase space of the microscopic state variables for the underlying Markovian model of $\mathcal{S}$ is spanned, therefore, by all the possible sets of k^*_{max} *streak bits*, $X \equiv \{s_1, s_2, \ldots, s_{k^*_{\mathrm{max}}}\}$, where

$$s_i = \begin{cases} 1, & \text{if the } i\text{th streak channel is active} \\ 0, & \text{otherwise.} \end{cases} \tag{4.7}$$

To make the concept clear, referring back to Fig. 5(b), we encode the microstate there exemplified as the set of streak bits

$$s_1 = s_2 = s_5 = s_6 = s_7 = s_9 = 0,$$
$$s_3 = s_4 = s_8 = s_{10} = 1. \tag{4.8}$$

We postulate now that the time evolution of the microscopic states X is produced from the independent fluctuations of streak bits, which have persistence probabilities that depend on the total number of active streak channels, that is, the OS label m. In this way we define q_m and p_m to be the persistence probabilities for any given streak bit to keep its value 0 or 1, respectively, along subsequent sPIV snapshots. There are, thus, four different types of streak bit flips, which appear in different occurrence numbers for a given OS mode transition, as summarized in Table I.

The parameters reported in Table I are related to the OS mode transition $m \to m'$, where $m = n_3 + n_4$ and $m' = n_2 + n_4$. The transition probability between any specific pair of associated microstates is, as a consequence, $q_m^{n_1}(1 - q_m)^{n_2}(1 - p_m)^{n_3} p_m^{n_4}$. Taking into account, furthermore, the role of degeneracy factors, we may write the transition probability $T_{m'm}$ between the OS modes m

TABLE I. Definition of the four possible transition types for the streak channel states together with the notations for their occurrence numbers and individual transition probabilities. $m = n_3 + n_4$ labels the OS mode.

Transition type	No. of streak channels	Transition probability
$0 \to 0$	n_1	q_m
$0 \to 1$	n_2	$1 - q_m$
$1 \to 0$	n_3	$1 - p_m$
$1 \to 1$	n_4	p_m

and m' as

$$T_{m'm} = \binom{k_{\max}^*}{m}^{-1} \sum_{n_1=0}^{k_{\max}^*} \sum_{n_2=0}^{k_{\max}^*} \sum_{n_3=0}^{k_{\max}^*} \sum_{n_4=0}^{k_{\max}^*} \delta\left(\sum_{i=1}^4 n_i, k_{\max}^*\right) \delta(n_3 + n_4, m) \delta(n_2 + n_4, m')$$
$$\times \, \Omega_1 \Omega_2 \Omega_3 q_m^{n_1} (1 - q_m)^{n_2} (1 - p_m)^{n_3} p_m^{n_4}, \tag{4.9}$$

where

$$\Omega_1 = \binom{k_{\max}^*}{n_1}, \tag{4.10}$$

$$\Omega_2 = \binom{k_{\max}^* - n_1}{n_2}, \tag{4.11}$$

$$\Omega_3 = \binom{k_{\max}^* - n_1 - n_2}{n_3}. \tag{4.12}$$

Using, from now on, $k_{\max}^* = 10$, the Markovian model just introduced may not appear very phenomenologically attractive at first glance, since $T_{m'm}$ is parametrized by a large number of unknown parameters ($q_0, q_1, \ldots, q_9$ and $p_1, p_2, \ldots, p_{10}$). Note, however, that there are, in principle, 90 independent entries in the empirical transition matrix (the one derived from the sPIV measurements), so the model is rather underdetermined (as we would expect for a phase-space reduced description of turbulent fluctuations).

Instead of attempting to provide a detailed and computationally costly model of the empirical transition matrix, we address a much simpler approach, where we focus on the asymptotic probability eigenvector of the modeled transition matrix,

$$\mathbb{P} = (P_1, P_2, \ldots, P_{10}), \tag{4.13}$$

which satisfies $\mathbb{T}\mathbb{P} = \mathbb{P}$, that is, $\sum_{m=0}^{10} T_{m'm} P_m = P_{m'}$. Here P_m is the probability that the OS mode m be observed in the statistically stationary regime. In an analogous way, denoting by $\mathbb{P}_\infty$ the empirical probability vector, determined from the sPIV measurements, we are interested to find the set of probabilities q_m and p_m that minimize the quadratic error

$$d(\{q_m\}, \{p_m\}) \equiv ||\mathbb{P} - \mathbb{P}_\infty||^2. \tag{4.14}$$

While, as already commented, the original problem is underdetermined, the optimization scheme related to Eq. (4.14) is not: as a matter of fact, we would have to model the nine independent probability entries of (4.13) by means of the 20 probability parameters q_m and p_m. To reduce this large overdeterminacy, we rely on a few phenomenological inputs:

(i) We assume that we can model the observed coherence (time persistence) of low-speed streaks by a single mode-independent and not small probability parameter p, where $p = p_2 = p_3 = \cdots = p_{10}$.

(ii) P_0 turns out to be negligible, so we suppress transitions from the OS mode $m = 1$ to $m = 0$, by imposing that $p_1 = 1$ (other transitions to the mode $m = 0$ from modes $m \neq 1$ are possible, but they are of $O[(1 - p)^2]$).

Therefore, we end up with 11 parameters ($q_0, q_1, \ldots, q_9$ and p) to locate the minimum value of (4.14). The result is a slightly overdetermined system, but if besides $\mathbb{P}_\infty$, the correlation functions $F(t - t')$ and $G(t - t')$ turn out to be well reproduced with the same set of probability parameters, as an extra bonus, then the model can be taken as physically appealing. That is the heuristic setup that we have in mind.

We have resorted to a straightforward Monte Carlo procedure to obtain the set of q_m that minimizes (4.14) for various fixed values of p. We find, as shown in Fig. 6, that the quadratic error quickly drops for $p \geqslant 0.85$. The modeled asymptotic probabilities for the occurrence of OS modes are excellently compared, in Fig. 7, to the empirical ones for the cases $p = 0.86$ and $p = 0.95$.
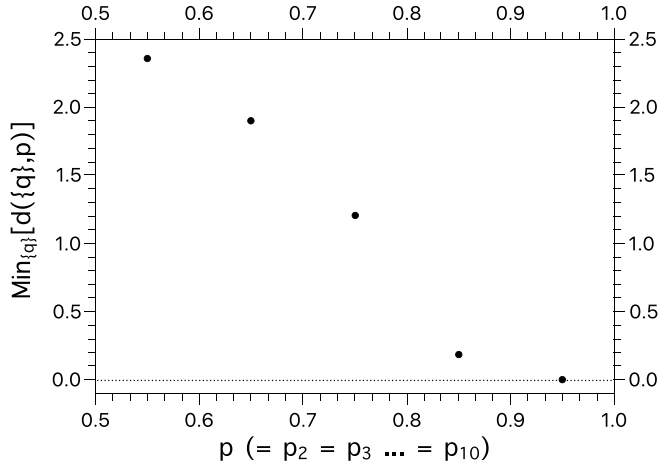
FIG. 6. Minimization of the quadratic distance $d(\{q\}, p)$ for various values of p.

These are the values of p that lead to good accounts of $F(t - t')$ and $G(t - t')$, as reported in Fig. 8. The related values of the probabilities q_m are listed in Table II. Even if a point of subjective concern, the uncertainty of about 10% in the definition of p should be taken as relatively small, *vis-à-vis* the model's accuracy in predicting the decaying profiles of the OS correlation functions.

Also evidenced in the inset Fig. 8 is the exponential decay profile of the modeled $G(t - t')$ for time intervals larger than δt. At present, this point rests as a prediction of the modeling scenario introduced in this work. A more extensive study of larger time series is necessary to settle the issue, since accidentally the observed sudden undersampling of the time series for larger decimations of $\mathcal{S}$ takes place around the expected crossover timescale δt.

The physical picture that emerges from our analysis is that the OSs are packed as chains of low-speed streaks and vortical structures which are strongly correlated within sizes that scale with the pipe's diameter, although they are merged along the entire turbulent flow. They can be taken as the analogous of the hairpin vortex packets of turbulent boundary layers, evidenced from both visual inspections and statistical treatments [15–17]. The relevant phenomenological difference, however, is that pipe flow is confined, so that vortex packets are likely to mix and interact in a more complex
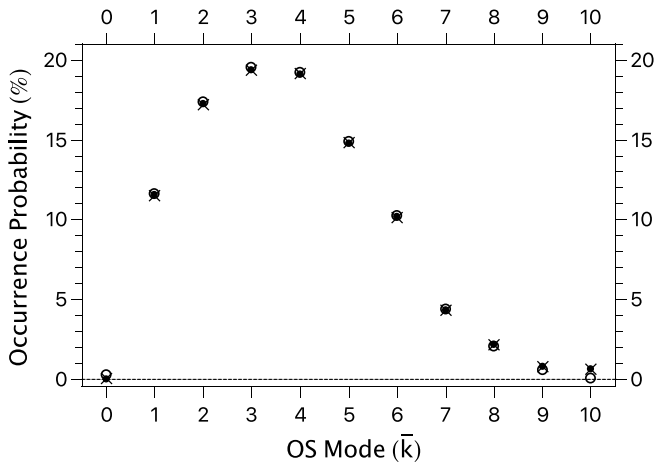

FIG. 7. Occurrence probability of OS modes obtained from the experiment (dots) and from the stochastic model (open circles: $p = 0.86$; crosses: $p = 0.95$), defined by the transition matrix elements (4.9).
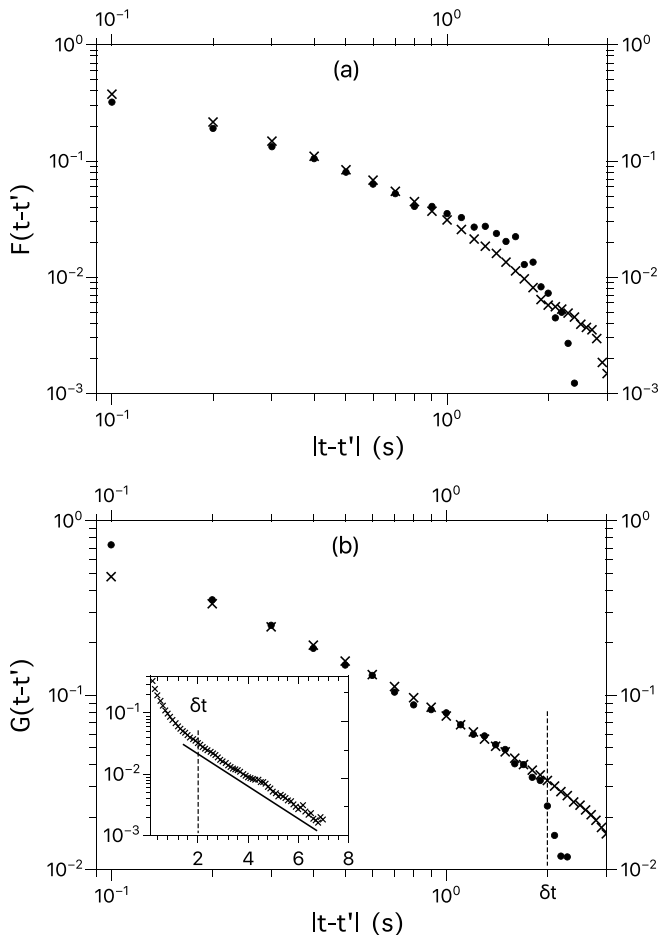
FIG. 8. Empirical (dots) and modeled (crosses) correlation functions $F(t - t')$ and $G(t - t')$. Crosses refer in (a) and (b), respectively, to modeling parameters $p = 0.86$ and $p = 0.95$. The semilog plot in the inset of (b) indicates the simple exponential form of $G(t - t')$ at large enough $|t - t'|$.

way as they grow from the pipe walls towards the bulk of the flow. In this situation, at variance with the case of turbulence boundary layers, the well-developed vortex packets lose their spatial patterns but are nevertheless expected to leave a trace of their presence in the self-similar behavior of the correlation functions given in Fig. 4.

V. CONCLUSIONS

We have investigated the stochastic properties of the non-Markovian OS mode transitions in a turbulent pipe flow, recovering them as a surjective mapping of a lower-level Markov process. The

TABLE II. List of probabilities q_m which describe the persistence of inactive streak channels for the cases $p = 0.86$ and $p = 0.95$.

p	q_0	q_1	q_2	q_3	q_4	q_5	q_6	q_7	q_8	q_9
0.86	0.53	0.96	0.95	0.92	0.92	0.85	0.95	0.75	0.86	1.0
0.95	0.22	0.98	0.98	0.97	0.97	0.96	0.97	0.93	0.94	0.49

essential idea that underlies the model construction is that a given OS mode may be associated with several spatial arrangements of its low-speed streaks into a fixed number of "streak channels" which azimuthally partition the pipe's cross section.

As is commonly known, a given discrete stochastic process may be not Markovian due to the fact that if the timescales under scrutiny are too short, the dynamical evolution of the microscopic variables may depend on the details of their specific phase-space trajectories. However, it is worth stressing—and this is at the core of our discussion—that even in the absence of microscopic memory effects, transitions between the chosen stochastic variables may not satisfy the Chapman-Kolmogorov equation if they are not uniquely defined from the underlying microscopic state variables [18].

We have found, accordingly, that a lower-level Markov model can account for the scaling behavior of specifically introduced correlation functions of OS mode transitions. Further work is in order, not only to enlarge the size of sPIV ensembles, but also to address, in an analytical way, the very unexpected self-similar dynamics of the OS mode transitions. Such improvements could lead to more accurate estimates of the transition probabilities given in Table II. It is likely that the uncertainty in the definition of the probability parameters reported in that table has to do with the assumption of the independency of p upon the OS modes and/or with the specific optimization procedure we have carried out for the evaluation of the $q's$. These are, surely, points for alternative formulations in additional studies of the OS mode transitions.

It turns out, furthermore, that the self-similar scaling range of the recurrent OS transitions can be interpreted as the statistical signature of finite-sized OS packets along the pipe flow, correlated at integral length scales (i.e., the pipe's diameter). In contrast with the geometric self-similar structure of hairpin packets in turbulent boundary layers [15–17], a phenomenological understanding of the scale-invariant behaviors given in Fig. 4 is not clear yet. It is possible that the origin of self-similarity here, analogously to what is verified in other nonlinear processes, relies on the fact that the OS mode transitions induced by flow instabilities occur in the form of direct and inverse cascades across their associated length scales.

An interesting theoretical direction to pursue, in this connection, is related to the use of instanton techniques [19] to evaluate the transition probabilities between unstable flow configurations as are the OS modes (which in a first approximation can be tentatively modeled as the appropriately rescaled traveling wave solutions of [5,6]). In the turbulence or transitional context, instantons are taken, respectively, as extreme events or flow configurations that dominate the probability measures in the weak coupling limit. They have been successfully applied to a number of fluid dynamic problems, as in geophysical models, homogeneous turbulence, and the laminar-turbulent transition in shear flows [20–22].

We conclude by noting that the findings here presented are likely to add relevant phenomenological information to the discussion of fundamentally important issues in pipe flow turbulence, as drag control and particle-laden dynamics, once they are closely connected to the statistical features of near-wall coherent structures [23–28].

ACKNOWLEDGMENTS

APPENDIX: CHAPMAN-KOLMOGOROV ANALYSIS OF THE OS MODE TRANSITIONS

While it is not possible to conclude, in general, if a given finite time series is a Markov chain, one may check whether the Chapman-Kolmogorov (CK) equation holds for it, a necessary condition for a stochastic process to be Markovian [29].
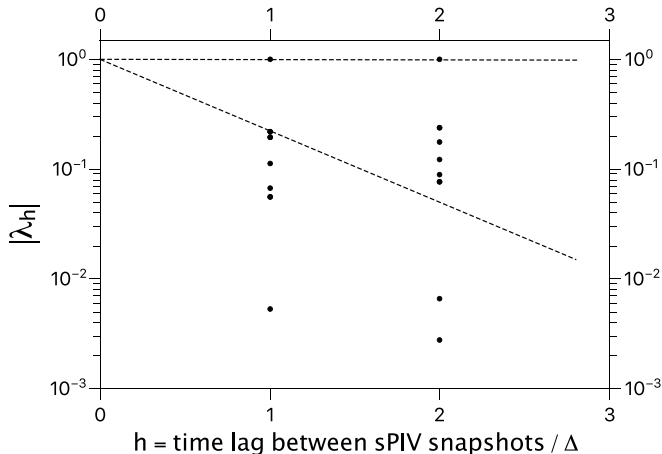
FIG. 9. Eigenvalues of the probability transition matrices for the original process ($h = 1$) and a decimated one ($h = 2$). The dashed lines should intercept eigenvalue pairs if $\mathcal{S}$ were a Markovian process. In other words, we find that the transition probability matrix of the decimated process is not given as the square of the transition probability matrix of the original process, as would be expected for a Markovian process.

In the particular case of (2.3), the CK equation would imply that the eigenvalues of the transition probability matrix for OS modes separated by the time interval $h\Delta$ can be represented in some arbitrary ordering as the set of powers $\{\lambda_1^h, \lambda_2^h, \ldots, \lambda_{k_{\max}^*}^h\}$. A straightforward computation of the transition matrix eigenvalues for the cases $h = 1$ and $h = 2$ indicates, however, that $\mathcal{S}$ is not Markovian; see Fig. 9.

[1] O. Reynolds, An experimental investigation of the circumstances which determine whether the motion of water in parallel channels shall be direct or sinuous and of the law of resistance in parallel channels, Philos. Trans. R. Soc. London **174**, 935 (1883).

[2] B. Hof, C. W. H. van Doorne, J. Westerweel, F. T. M. Nieuwstadt, H. Faisst, B. Eckhardt, H. Wedin, R. R. Kerswell, and F. Waleffe, Experimental observation of nonlinear traveling waves in turbulent pipe flow, Science **305**, 1594 (2004).

[3] T. M. Schneider, B. Eckhardt, and J. Vollmer, Statistical analysis of coherent structures in transitional pipe flow, Phys. Rev. E **75**, 066313 (2007).

[4] D. J. C. Dennis and F. M. Sogaro, Distinct Organizational States of Fully Developed Turbulent Pipe Flow, Phys. Rev. Lett. **113**, 234501 (2014).

[5] H. Faisst and B. Eckhardt, Traveling Waves in Pipe Flow, Phys. Rev. Lett. **91**, 224502 (2003).

[6] H. Wedin and R. R. Kerswell, Exact coherent structures in pipe flow: Travelling wave solutions, J. Fluid Mech. **508**, 333 (1999).

[7] Following [4], we adopt the use of "organizational states" instead of "traveling waves" to refer to the coherent structures observed in a turbulent pipe flow. The rationale behind this lexical choice is to emphasize the phenomenological distinction between the flow regimes of high and low/transitional Reynolds numbers.

[8] J. Gibson, J. Halcrow, and Cvitanović, Visualizing the geometry of state space in plane Couette flow, J. Fluid Mech. **611**, 107 (2008).

[9] J. Moehlis, H. Faisst, and B. Eckhardt, Periodic orbits and chaotic sets in a low-dimensional model for shear flows, SIAM J. Appl. Dyn. Syst. **4**, 352 (2005).

[10] N. B. Budanur, K. Y. Short, M. Farazmand, A. P. Willis, and P. Cvitanović, Relative periodic orbits form the backbone of turbulent pipe flow, J. Fluid Mech. **833**, 274 (2017).

[11] G. Yalnız, B. Hof, and N. B. Budanur, Coarse Graining the State Space of a Turbulent Flow Using Periodic Orbits, Phys. Rev. Lett. **126**, 244502 (2021).

[12] E. Marensi, G. Yalnız, B. Hof, and N. B. Budanur, Symmetry-reduced dynamic mode decomposition of near-wall turbulence, J. Fluid Mech. **954**, A10 (2023).

[13] J. M. J. den Toonder and F. T. M. Nieuwstadt, Reynolds number effects in a turbulent pipe flow for low to moderate Re, Phys. Fluids **9**, 3398 (1997).

[14] R. Jäckel, B. Magacho, B. E. Owolabi, L. Moriconi, D. J. C. Dennis, and J. B. R. Loureiro, Coherent organizational states in turbulent pipe flow at moderate Reynolds numbers, Phys. Fluids **35**, 045127 (2023).

[15] R. J. Adrian, C. D. Meinhart, and C. D. Tomkins, Vortex organization in the outer region of the turbulent boundary layer, J. Fluid Mech. **422**, 1 (2000).

[16] K. T. Christensen and R. J. Adrian, Statistical evidence of hairpin vortex packets in wall turbulence, J. Fluid Mech. **431**, 433 (2001).

[17] R. Deshpande, C. M. de Silva, and I. Marusic, Evidence that superstructures are concatenations of self-similar coherent motions in high Re_τ boundary layers, arXiv:2210.06039.

[18] N. G. van Kampen, *Stochastic Processes in Physics and Chemistry* (Elsevier, Amsterdam, 2007).

[19] T. Grafke, R. Grauer, and T. Schäfer, The instanton method and its numerical implementation in fluid mechanics, J. Phys. A: Math. Theor. **48**, 333001 (2015).

[20] J. Laurie and F. Bouchet, Computation of rare transitions in the barotropic quasi-geostrophic equations, New J. Phys. **17**, 015009 (2015).

[21] G. B. Apolinário, L. Moriconi, R. M. Pereira, and V. J. Valadão, Eddy-viscous modeling and the topology of extreme circulation events in three-dimensional turbulence, Phys. Lett. A **449**, 128360 (2022).

[22] S. Gomé, L. S. Tuckerman, and D. Barkley, Extreme events in transitional turbulence, Philos. Trans. R. Soc. A **380**, 20210036 (2022).

[23] H. Choi, P. Moin, and J. Kim, Active turbulence control for drag reduction in wall-bounded flows, J. Fluid Mech. **262**, 75 (1994).

[24] W. Schoppa and F. Hussain, A large-scale control strategy for drag reduction in turbulent boundary layers, Phys. Fluids **10**, 1049 (1998).

[25] I. Marusic, D. Chandran, A. Rouhi, M. K. Fu, D. Wine, B. Holloway, D. Chung, and A. J. Smits, An energy-efficient pathway to turbulent drag reduction, Nat. Commun. **12**, 5805 (2021).

[26] E. Gallorini, M. Quadrio, and D. Gatti, Coherent near-wall structures and drag reduction by spanwise forcing, Phys. Rev. Fluids **7**, 114602 (2022).

[27] G. Wang and D. Richter, Modulation of the turbulence regeneration cycle by inertial particles in planar Couette flow, J. Fluid Mech. **861**, 901 (2019).

[28] L. Brandt and F. Coletti, Particle-laden turbulence: Progress and perspectives, Annu. Rev. Fluid Mech. **54**, 159 (2022).

[29] E. Çirlan, *Introduction to Stochastic Process* (Dover, Mineola, New York, 1975).